Experimental Filter Comparison of an Acoustic Positioning System for Unmanned Underwater Navigation

Sørensen, Fredrik Fogh; von Benzon, Malte; Pedersen, Simon; Liniger, Jesper; Schmidt, Kenneth; Klemmensen, Sigurd

Published in:
IFAC-PapersOnLine

DOI (link to publication from Publisher):
10.1016/j.ifacol.2022.11.328

Publication date:
2022

Document Version
Publisher's PDF, also known as Version of record

Available online at www.sciencedirect.com

ScienceDirect

IFAC Papers Online CONFERENCE PAPER ARCHIVE

IFAC PapersOnLine 55-36 (2022) 25–30

Experimental Filter Comparison of an Acoustic Positioning System for Unmanned Underwater Navigation

Fredrik Fogh Sørensen [*,**], **Malte von Benzon** [**], **Simon Pedersen** [**], **Jesper Liniger** [**], **Kenneth Schmidt** [**], **Sigurd Klemmensen** [***]

[*] *Corresponding author. E-mail: ffso@energy.aau.dk).*
[**] *AAU Energy, Aalborg University, Niels Bohrs Vej 8, DK-6700 Esbjerg, Denmark*
[***] *SubC Partner, 6700 Esbjerg, Denmark*

Abstract: The demand for Unmanned Underwater Vehicles (UUVs) for various operations has increased. Automating these operations requires good knowledge of the location of the UUV. This study investigates the filter lag in the commercial low-cost Underwater GPS Explorer Kit, a short baseline (SBL) from Water Linked. Furthermore, different filters are designed in an attempt to minimize the filter lag. Minimizing the lag is beneficial for real-time navigation, as delays have a negative impact on stability. Three different filters are designed; a model-free simple moving average (SMA) filter, a Kalman filter (KF) based on a constant velocity motion model, and lastly, an unscented Kalman filter (UKF) based on the non-linear model derived from the robot's dynamics. A large filter lag is found in the original filter; however, it can be concluded that a model-based filter with knowledge of the system dynamics can be used for minimizing the filter lag.

Keywords: Filter, Kalman Filter, AUV, ROV, Underwater Robotics, Time Delay,

1. INTRODUCTION

Over the last decade, there has been an increasing demand for Unmanned Underwater Vehicles (UUVs) for operations, such as seabed mapping, harbor monitoring, and offshore maintenance. One requirement for completing such operations is accurate localization (Yang and Huang (2017); Mai et al. (2016)). Unlike land and aerial vehicles, underwater vehicles cannot utilize the Global Navigation Satellite System (GNSS) due to radio waves' rapid attenuation in water (Paull et al. (2014)). According to Ribas et al. (2012), most underwater vehicles rely on dead-reckoning. However, these estimates are subject to drift and must use other techniques to bound the position error. The Absolute Acoustic Positioning System (AAPS) is commonly used, especially the Long Base Line (LBL). However, LBL is costly and demanding to deploy. To mitigate issues of LBL, other technologies such as Short Base Line (SBL) and Ultra Short Base Line (USBL) can be used for vehicle tracking (Ribas et al. (2012)). However, good control performance requires accurate and reliable feedback Kinsey et al. (2006). Especially, when performing operations near structures where collision are to be avoided, like during cleaning and visual inspection tasks. In such cases, sensor accuracy, resolution, and small measurement delays are more crucial than for long-distance navigation (Pedersen et al. (2022)).

When an AAPS is used for real-time navigation, the delay imposed by the acoustics has to be handled properly; otherwise, the delay might result in errors Ribas et al. (2012). Different ways to handle the sensor delay are proposed by Mandt et al. (2001). The most accurate method proposed is resetting navigation and filtering every time a delayed measurement arrives. Repeatedly recalculating the filtering is computationally demanding, especially for extensive sensor delay (Mandt et al. (2001)). In Jørgensen et al. (2020), a short baseline system with three receivers were used to aid the inertial measurement unit (IMU) in estimating both the position and attitude of an ROV. The results show that the proposed observer performance is close to the optimal non-implementable filter, which uses Qualisys underwater camera positioning system measurements.

The Water Linked underwater global positioning system, which is an SBL, differs from other industrial systems by its price, as this system can be acquired for less than $7000. Beside the low cost, the UGPS is easy integrable with the BlueROV2 (See WaterLinked (2022)) which is widely used research projects due to its affordable price (Wallen and Song (2019); Manzanilla et al. (2019)). Therefore, this SBL has interesting research capabilities if the measurements can be used as feedback. In Pedersen et al. (2019), an SBL system from Water Linked (Underwater GPS Explorer Kit) were used for real-time navigation. A varying measurement delay of 2.00 ± 0.55 sec was discovered. Despite the varying delay, a Smith-predictor, which assumes fixed delay, was developed to eliminate the effects of the delay. However the predictores feedback was not sufficient for the developed position controller. In Pedersen et al. (2019) it was not investigate how much of the discovered delay was sensor induced and filter induced; this needs to be investigated in order to tell whether an improved filter can improve the performance of the feedback.

In this study, the Water Linked SBL system is investigated regarding measurement delay. The filter lag imposed by the manufacturer's original filter is investigated through experimental tests. Furthermore, three filters are designed with the

10.1016/j.ifacol.2022.11.328

goal of minimizing the filter lag. The filters designed vary in computational demand from a Simple Moving Average (SMA) filter to Kalman Filter (KF) and, lastly, an Unscented Kalman Filter (UKF). The filter comparison will be evaluated based on filter-induced lag and delay.

2. SYSTEM DESCRIPTION

The SBL system used in this study is the UnderWater GPS Explorer Kit (UGPS) from Water Linked. It must be noted that Water Linked has revised this system; however, the revised system needs a hardware change, and is not used in this study; therefore, better performance might be experienced, if using the revised system. The UGPS consists of a topside box, four receivers (seen in Fig. 1b), and one locator, which is mounted on the ROV as shown in Fig. 1a.

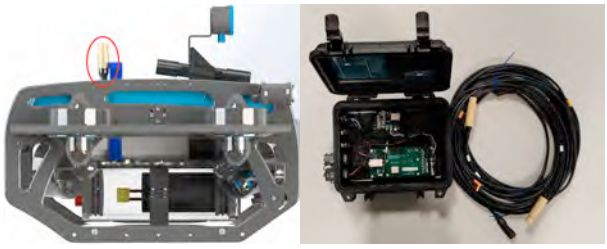

(a) BlueROV with locator mounted on top (see red circle).

(b) Underwater GPS Explorer Kit, the topside box with receivers.

Fig. 1. Underwater GPS Explore Kit from Water Linked.

The SBL system is tested in a pool with a diameter of 6.1 m and a depth of 1.15 m. The small size results in acoustic signals are inevitably reflected from the pool walls, which may influence the delay's magnitude and the precision of the location's signal. Hence, tests in open waters might show different results.

When placing the receivers, it was observed that their location greatly impacted how the system performed. Through experiments, it was found that the best configuration was to place the receivers aligned with the North and East axis, as seen in Fig. 2.

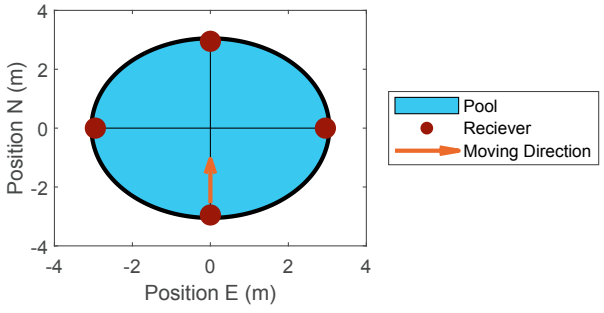

Fig. 2. Receiver setup. The red dots are the location of the four receivers, and the black circle illustrates the pool. The orange arrow shows the direction the ROV was towed in the experiments.

3. MODELING

In section 5 model-based filters are designed, therefore a model is required. The modeling of the ROV is based on Fossen's representation of underwater vehicles shown in Fossen (2011), and the parameters have been determined through a combination of experiments and can be found in Sørensen et al. (2022) and more details on the parameters can be found in the paper by Benzon et al. (2021) where the same platform has been used.

The governing equations are given by.

$$\dot{\boldsymbol{\eta}} = \boldsymbol{J}(\boldsymbol{\eta})\boldsymbol{\nu} \tag{1}$$

$$\boldsymbol{M}\dot{\boldsymbol{\nu}} + \boldsymbol{C}(\boldsymbol{\nu})\boldsymbol{\nu} + \boldsymbol{D}(\boldsymbol{\nu})\boldsymbol{\nu} + \boldsymbol{g}(\boldsymbol{\eta}) = \boldsymbol{\tau} \tag{2}$$

where $\boldsymbol{\eta} = [N, E, D, \phi, \theta, \psi]^T$ is a combination of world coordinates and Euler angles defined in the NED frame. $\boldsymbol{\nu} = [u, v, w, p, q, r]^T$ is the body-fixed velocity vector. In Fig. 3 both the NED and body-fixed frame definitions are shown.

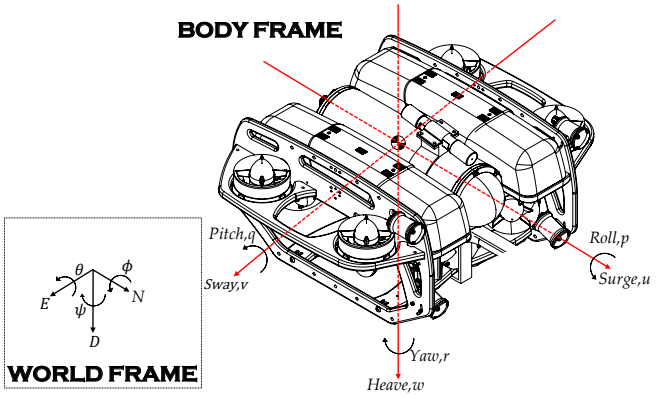

Fig. 3. Figure from Benzon et al. (2021). BlueROV2 with frame-definitions.

$\boldsymbol{J}(\boldsymbol{\eta})$ is the rotation matrix between the NED and body-fixed frame. For the external forces $\boldsymbol{\tau} = [\tau_1, \tau_2, \tau_3, \tau_4, \tau_5, \tau_6]^T$, which is the input given in forces τ_1, τ_2, τ_3 and torques τ_4, τ_5, τ_6.

The rest of the variables in (1) and (2) can be found in section 3 in Sørensen et al. (2022).

To get a mathematical expression for the acceleration, (2) is solved as an inverse problem with respect to $\dot{\boldsymbol{\nu}}$.

$$\dot{\boldsymbol{\nu}} = \boldsymbol{M}^{-1}\left(\boldsymbol{\tau} - \boldsymbol{C}(\boldsymbol{\nu})\boldsymbol{\nu} - \boldsymbol{D}(\boldsymbol{\nu})\boldsymbol{\nu} - \boldsymbol{g}(\boldsymbol{\eta})\right) \tag{3}$$

Equation (3) can then be formulated as a vector of non-linear functions.

$$\boldsymbol{f}(\boldsymbol{\eta}, \boldsymbol{\nu}, \boldsymbol{\tau}) = [\dot{u}(\boldsymbol{\eta}, \boldsymbol{\nu}, \boldsymbol{\tau}), \dot{v}(\boldsymbol{\eta}, \boldsymbol{\nu}, \boldsymbol{\tau}), \dot{w}(\boldsymbol{\eta}, \boldsymbol{\nu}, \boldsymbol{\tau}), \dot{p}(\boldsymbol{\eta}, \boldsymbol{\nu}, \boldsymbol{\tau}), \dot{q}(\boldsymbol{\eta}, \boldsymbol{\nu}, \boldsymbol{\tau}), \dot{r}(\boldsymbol{\eta}, \boldsymbol{\nu}, \boldsymbol{\tau})]^T \tag{4}$$

The non-linear model is used for filter design section 5.

4. SENSOR DELAY INVESTIGATION

The time delay of the SBL system is experimentally investigated. First, the time delay of the raw signal was determined by comparing the response from the onboard IMU and the raw signal from the SBL system. A similar test was carried out in Pedersen et al. (2019).

The experiment shows that the raw signal is delayed by approximately 1.5 sec as seen in Fig. 4. This is in the same range as found in Pedersen et al. (2019). Therefore it is assumed that the sensor delay of 2.00 ± 0.55 sec still applies.

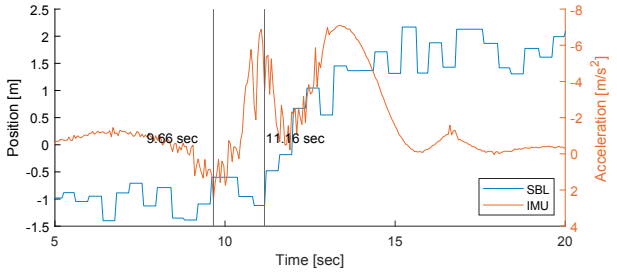

Fig. 4. The experiment showing the response from the accelerometer and the raw signal from the SBL system when the ROV is surged.

The experiment cannot determine whether the delay is sensor induced or filter induced. To investigate the filter lag an alternative experiment is conducted using an encoder for measuring the ROV travel directly. The encoder signal is integrated to obtain the ROV travel. This test shows the filter lag as the raw position and filtered position measurements are logged simultaneously by the SBL system. The test setup is illustrated in Fig. 5.

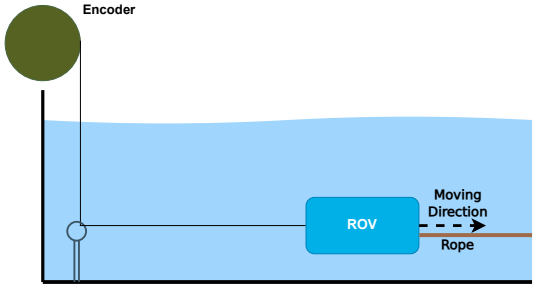

Fig. 5. Illustration of the test setup. The green circle is a spool, with an encoder attached to measure the angular velocity.

The results from the direct travel measurement can be seen in Fig. 6.

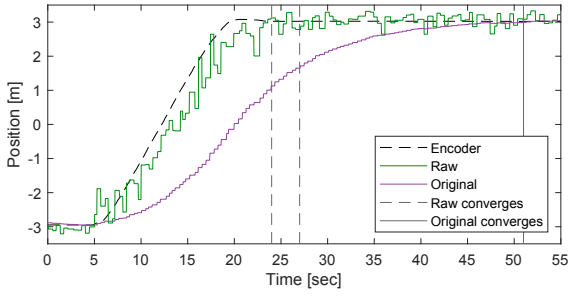

Fig. 6. Comparison of the integrated encoder signal, the raw SBL system signal and original Kalman filter output.

The comparison of the raw signals and the original Kalman filter is shown in Fig. 6 and shows the filter successfully reduces the noise but meanwhile imposes further lag than the raw signal.

The time between the raw signal and the filtered signal converges was determined to be between 24 sec to 27 sec, as it was hard to determine an exact value due to large variations in the raw signal. The ROV has a top speed of 0.73 m sec^{-1} (Benzon et al. (2021)), and it will be able to move more than 10 m before the SBL measures the location. This is clearly a problem for navigation in small operational areas, and a reduction in filter lag is demanded to have a useful feedback signal.

5. FILTER DESIGN

Three filters are designed to investigate if the original KF-generated signal can be improved. The first filter is a model-free filter with low computational effort, which in this case is an SMA, then a KF is designed, which uses a linear model. The KF uses only the sensor measurement y, with the assumption that measurement noise is Gaussian (this has been verified through steady-state tests), and the previous estimated state vector $\hat{x}$, to predict the next state estimates. Lastly, an UKF is designed, which uses the non-linear model. The UKF uses both the sensor output y, the previous estimated state vector $\hat{x}$, and the input to the system τ_1. The UKF is chosen over an extended Kalman filter (EKF), as the UKF reduces the linearization errors compared to the EKF but comes at the cost of extra computational effort (Paull et al. (2014)).

5.1 Simple Moving Average

The SMA has the advantage that it is a single line operation with simple math operators; this means that it has a low computational cost compared to the other filters designed in this study.

The moving average uses the average value of the measurements y over a fixed window of measurements. It is formulated as,

$$y_{SMA} = \frac{1}{m} \sum_{i=n-m+1}^{n} y_i \tag{5}$$

where y_i is the measurement, m is the window size, n is the total number of measures, and y_{SMA} is the filtered measurement.

m determines how fast the filter reacts to changes; a large m makes changes appear slower but reduces noise. In this study $m = 10$, which was found by evaluating the trade-off between responsiveness and smoothness.

5.2 Kalman Filter

For the KF, a simple constant velocity motion model is used.

$$N_{k+1} = N_k + \dot{N}_k \delta t \tag{6}$$

where N_k is position and $\dot{N}_k$ is the velocity in the the NED frame, while δt is the time step between the positions.

When rewriting the constant velocity motion equation to a discrete state-space equation with states $\boldsymbol{x} = [N,\ \dot{N}]^T$, the system matrix becomes

$$\boldsymbol{A} = \begin{bmatrix} 1 & \delta t \\ 0 & 1 \end{bmatrix} \tag{7}$$

The output matrix is the measured states, which is the position N.

$$\boldsymbol{C} = [\,1\ 0\,] \tag{8}$$

KF is a linear optimal state estimation method and is often used to remove sensor Gaussian noise from raw sensor data (Park et al. (2019)). KF consists of two steps; the first step is the time update, in which a linear model is used to predict the following state values. The second step is the measurement update, which uses an actual measurement to correct the predicted state.

The calculation for KF is shown in (9)-(13)

Time Update

$$\hat{\boldsymbol{x}}_{k+1|k} = \boldsymbol{A}\hat{\boldsymbol{x}}_{k|k} \tag{9}$$

$$\boldsymbol{P}_{k+1|k} = \boldsymbol{A}\boldsymbol{P}_{k|k}\boldsymbol{A}^T + \boldsymbol{Q} \tag{10}$$

Measurement Update

$$\boldsymbol{K} = \boldsymbol{P}_{k+1|k}\boldsymbol{C}^T\left(\boldsymbol{C}\boldsymbol{P}_{k+1|k}\boldsymbol{C}^T + R\right)^{-1} \tag{11}$$

$$\hat{\boldsymbol{x}}_{k+1|k+1} = \hat{\boldsymbol{x}}_{k+1|k} + \boldsymbol{K}\left(y_k - \boldsymbol{C}\hat{\boldsymbol{x}}_{k+1|k}\right) \tag{12}$$

$$\boldsymbol{P}_{k+1|k+1} = (\boldsymbol{I} - \boldsymbol{K}\boldsymbol{C})\boldsymbol{P}_{k+1|k} \tag{13}$$

where $\hat{\boldsymbol{x}}$ is the state estimate $[\hat{N}, \hat{N}]^T$, y is the SBL raw measurement, $\boldsymbol{Q}$ is the process noise, R is the sensor noise, $\boldsymbol{P}_{k|k}$ is the state co-variance, and $\boldsymbol{K}$ is the Kalman gain. $\boldsymbol{Q}$, R, and the initial $\boldsymbol{P}_{k|k}$ have to be determined. The subscript k is the discrete sample number, when multiple updates are done to a single variable at one time step, the subscript $k|k$ are used, where each represent a change in the variable (time Update and measurement update).

$\boldsymbol{Q}$ is in many cases represented as an acceleration disturbance to the system (Kazimierski and Zaniewicz (2021)).

$$\boldsymbol{Q} = \boldsymbol{G}\boldsymbol{G}^T\sigma_a^2 \tag{14}$$

where $\boldsymbol{G}$ is a 2x2 diagonal matrix, whose elements are $diag(0.5\delta t, \delta t)$, and σ_a is the standard deviation of the disturbance represented as acceleration. In this study σ_a is chosen to be 5 % of the maximum thrust force in surge, which is $\tau_{1,max} =$ 86 N Benzon et al. (2021), which means $\sigma_a = 0.217\,\mathrm{m\,sec^{-1}}$.

$$\boldsymbol{Q} = \begin{bmatrix} 0.0144^2 & 0 \\ 0 & 0.0789^2 \end{bmatrix} \tag{15}$$

R is determined by calculating the standard deviation of steady-state raw measurements from the SBL system.

$$R = 0.3557^2 \tag{16}$$

$\boldsymbol{P}$ is determined by the maximum difference between the initial state estimate $\hat{\boldsymbol{x}}_0$ and the initial true state $\boldsymbol{x}_0$.

$$\boldsymbol{P} = (\hat{\boldsymbol{x}}_0 - \boldsymbol{x}_0)(\hat{\boldsymbol{x}}_0 - \boldsymbol{x}_0)^T\boldsymbol{I} \tag{17}$$

As the ROV always starts with zero velocity, the velocity uncertainty is small. As the ROV is placed in a known position in these experiments, the position variation is small as well.

$$\boldsymbol{P} = \begin{bmatrix} 0.1^2 & 0 \\ 0 & 0.1^2 \end{bmatrix} \tag{18}$$

5.3 Unscented Kalman Filter

The UKF builds upon the Unscented Transform (UT), which is a method for calculating statistics of a stochastic variable undergoing a non-linear transformation.

The non-linear model used for the UKF is the model derived in section 3, and the states for is $x = [\eta,\ \nu]^T$. The non-linear discretized model using forward Euler can be described by

$$\begin{bmatrix} \boldsymbol{\eta}_{k+1} \\ \boldsymbol{\nu}_{k+1} \end{bmatrix} = \begin{bmatrix} \boldsymbol{\eta}_k + \boldsymbol{J}(\boldsymbol{\eta}_k)\boldsymbol{\nu}_k\delta t \\ \boldsymbol{\nu}_k + f(\boldsymbol{\eta}_k, \boldsymbol{\nu}_k, \boldsymbol{\tau}_k)\,\delta t \end{bmatrix} \tag{19}$$

where δt is the time step and k is the sample index.

However due to lack of reliable angular measurements and the fact that the experiments are only done in one direction (N), (19) is reduced to only concerning N by making the assumption the attitude of the ROV is constant and zero. Thereby $\boldsymbol{J}(\boldsymbol{\eta})$ becomes an identity matrix meaning $\boldsymbol{\eta}_{k+1} = \boldsymbol{\eta}_k + \boldsymbol{\nu}_k\delta t$. The model is further reduced to only concern N and u as for KF, meaning $x = [N,\ u]^T$.

The reduced non-linear model used in the UKF can thereby be described as.

$$\begin{aligned} \dot{u}(\boldsymbol{\eta}, \boldsymbol{\nu}, \boldsymbol{\tau}) = {} & 0.0504\tau_1 - 0.109sin(\theta) - 0.0504u \\ & (141.0|u| + 13.7) + 1.62rv - 1.04qw \end{aligned} \tag{20}$$

It is seen that the orientation and the angular velocity are present in the above equation. As these are assumed to be zero, these terms disappear. leaving (20) as the reduced model.

$$\dot{u}(u, \tau_1) = 0.0504\tau_1 - 0.0504u(141.0|u| + 13.7) \tag{21}$$

Moreover, since the ROV was towed in the experiments (see Fig 5), the surge force (thrust), normally stemming from the thrusters, is instead the applied force from the tow-rope. Since this force is not directly measured, the approximate applied velocity $\tilde{u}$ and acceleration $\dot{\tilde{u}}$ from the tow system is back-calculated from the encoder positions $d_{enc,k}$ and used to calculate the equivalent forces,

$$\tilde{u} = \dot{d}_{enc,k} = \frac{d_{enc,k} - d_{enc,k-1}}{\delta t_{enc}} \tag{22}$$

$$\dot{\tilde{u}} = \ddot{d}_{enc,k} = \frac{\dot{d}_{enc,k} - \dot{d}_{enc,k-1}}{\delta t_{enc}} \tag{23}$$

$$\tau_{1,k} = \frac{\dot{\tilde{u}}}{0.0504} + \tilde{u}(141.0|\tilde{u}| + 13.7) \tag{24}$$

where δt_{enc} is the sampling rate for the encoder. It must be noted that using this method for input estimation may provide a less realistic estimate than obtaining the input from the thruster input directly, as uncertainties in the thruster model are not included. Under normal operation the input to the UKF will be the thruster input given to the thrusters, not the encoder backcalculation as this is only present in this specific test setup.

The reduced non-linear model is discretized using forward Euler and describing position and velocity.

$$\boldsymbol{F}(\boldsymbol{x}_k, \tau_{1,k}) = \begin{bmatrix} N_k + u_k\delta t \\ u_k + \dot{u}(u_k, \tau_{1,k})\delta t \end{bmatrix} \tag{25}$$

where $\boldsymbol{x}_k$ is the state vector for the filter, which consists of the position and the velocity $\boldsymbol{x}_k = [N_k,\ u_k]^T$.

The statistical features of $\boldsymbol{x}_k$ are determined from the UT by forming sigma vectors $\boldsymbol{\chi}_i$ by the use of the state mean $\hat{\boldsymbol{x}}_{k|k}$ and its covariance $\boldsymbol{P}_{k|k}$. The calculation of the $\boldsymbol{\chi}_i$ can be seen in (29)-(31). The index i in $\boldsymbol{\chi}_i$ corresponds to $i = 0, .., 2n$, where n is the number of states.

By combining the UT and the KF theory, the UKF is designed. UKF works in 5 steps, one initial step and four recursive steps, which are recalculated at each time step.

Initial Calculations

$$W_0^m = \frac{\lambda}{\lambda + n} \tag{26}$$

$$W_0^c = W_0^m + \left(1 - \alpha^2 + \beta\right) \tag{27}$$

$$W_i^c = W_i^m = \frac{1}{2(\lambda + n)},\ (i = 1, \ldots, 2n) \tag{28}$$

W_i^m and W_i^c are weights used to normalize the the sigma points, where $\lambda = \alpha^2(k+n) - n$ is a scaling parameter, α describes the spread of the sigma points around the state estimate and is a small positive value. In this study $\alpha = 0.1$, β describes the distribution of state variables. $\beta = 2$ is optimal for Gaussian

distributions (Wan and Merwe (2000)). k is a secondary scale parameter and is usually set to zero (Li et al. (2015)). $\boldsymbol{P}_{k|k}$ is initialized as the expected variance between the true state and the estimated state vector; this is initialized with the same values as for the KF (see (18)).

Sigma Points Update

$$\boldsymbol{\chi}_0 = \hat{\boldsymbol{x}}_k \tag{29}$$

$$\boldsymbol{\chi}_i = \hat{\boldsymbol{x}}_k + \left(\sqrt{(n+\lambda)\boldsymbol{P}_{k|k}}\right)_i^T, \ (i = 1,\ldots,n) \tag{30}$$

$$\boldsymbol{\chi}_i = \hat{\boldsymbol{x}}_k - \left(\sqrt{(n+\lambda)\boldsymbol{P}_{k|k}}\right)_{i-n}^T, \ (i = n+1,\ldots,2n) \tag{31}$$

Time Update

$$\boldsymbol{\varepsilon}_i = F(\boldsymbol{\chi}_i), \ (i = 0,\ldots,2n) \tag{32}$$

$$\hat{\boldsymbol{x}}_{k+1|k} = \sum_{i=0}^{2n} W_i^m \boldsymbol{\varepsilon}_i \tag{33}$$

$$\boldsymbol{P}_{k+1|k} = \boldsymbol{Q} + \sum_{i=0}^{2n} W_i^c \left(\boldsymbol{\varepsilon}_i - \hat{\boldsymbol{x}}_{k+1|k}\right)\left(\boldsymbol{\varepsilon}_i - \hat{\boldsymbol{x}}_{k+1|k}\right)^T \tag{34}$$

Measurement Update

$$Z_i = [1 \ 0](\boldsymbol{\varepsilon}_i), \ (i = 0,\ldots,2n) \tag{35}$$

$$\hat{z} = \sum_{i=0}^{2n} W_i^m Z_i \tag{36}$$

$$\boldsymbol{P}_{zz} = \boldsymbol{R} + \sum_{i=0}^{2n} W_i^c \left(Z_i - \hat{z}_{k+1|k}\right)\left(Z_i - \hat{z}\right)^T \tag{37}$$

$$\boldsymbol{P}_{xz} = \sum_{i=0}^{2n} W_i^c \left(\boldsymbol{\varepsilon}_i - \hat{\boldsymbol{x}}_{k+1|k}\right)\left(Z_i - \hat{z}\right)^T \tag{38}$$

Filter Update

$$\boldsymbol{K} = \boldsymbol{P}_{xz}\boldsymbol{P}_{zz}^{-1} \tag{39}$$

$$\hat{\boldsymbol{x}}_{k+1} = \hat{\boldsymbol{x}}_{k+1|k} + \boldsymbol{K}(y_k - \hat{z}) \tag{40}$$

$$\boldsymbol{P}_{k+1|k+1} = \boldsymbol{P}_{k+1|k} + \boldsymbol{K}\boldsymbol{P}_{zz}\boldsymbol{K}^T \tag{41}$$

$\boldsymbol{Q}$, $\boldsymbol{R}$ and $\boldsymbol{P}_{k|k}$ equal to the once found for the KF as the same platform is used.

6. RESULTS

The three filters presented were implemented on the ROV and two towing tests was conducted. One test in which the ROV was towed from one side to the other, the results of this test can be seen in Fig. 7 and another test where the ROV was stopped three times, these results are shown in Fig. 9.

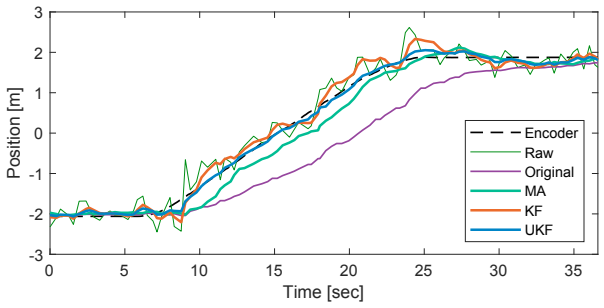

Fig. 7. Comparison of different filter algorithms applied on raw data from an SBL system.

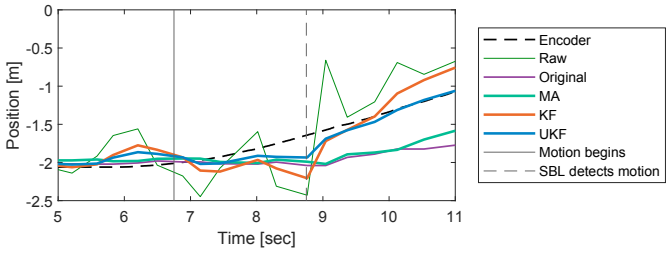

(a) Comparison of different filters when motion begins on same data-set as shown in Fig. 7.

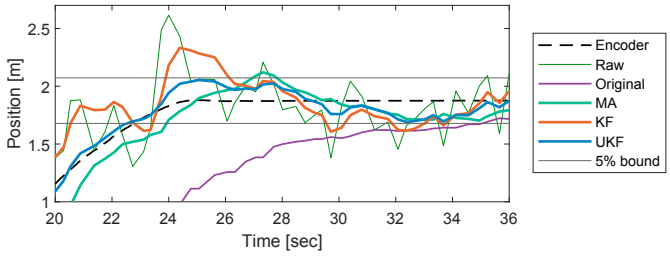

(b) Comparison of different filters when reaching the final location on same data-set as shown in Fig. 7. The 5 % bound is defined as ±5 % of the total distance traveled in regards the true position, according to the encoder measurement

Fig. 8. Areas of interest on the data-set shown on Fig. 7.

In Fig. 7 it can be seen that the original filter is expectedly lagging the true position (measured by the encoder). The three designed filters follow the true position with a smaller deviation than the original filter. The designed filters do not counter the sensor delay in the raw signal, which is clearly seen in Fig. 8a. From this figure it can also be seen that both the original filter and the MA lag behind the raw signal while the KF and UKF have better tracking on the true position.

From Fig. 8b it can be seen that the UKF reaches a bound within 5 % of the true position, according to the encoder measurement, at the same time as the encoder measurement reaches the position. MA has reached the bound 4.95 sec later, while the KF reaches the bound 10.9 sec after the true position due to an overshoot. The original filter shows no oscillations; however it reaches the bound 11.2 sec after the true measurement reaches its final position, which shows that the original filter is very conservative.

The test with three stops of a duration of 14 sec each (Seen in Fig. 9), shows that the original filter barely reaches the true location at each stop, before the ROV moves again. Another observation is that the SBL measurements have an offset at the first stop, the encoder measures the position to 0.08 m and the SBL measures approximately −0.18 m. This deviation is suspected to be caused by acoustic reflections from the walls of the pool. Tests in open waters could show different results. However, the test shows that the developed filters is on par with the raw signal, without noticeable lag compared to the original filter.

7. CONCLUSION AND FUTURE WORK

In this study, it is found that the manufacturer's original filter has a large filter lag, with convergence time between 24 sec to 27 sec. To investigate whether the filter lag could be reduced by alternative filters, three filters were designed and experimen-

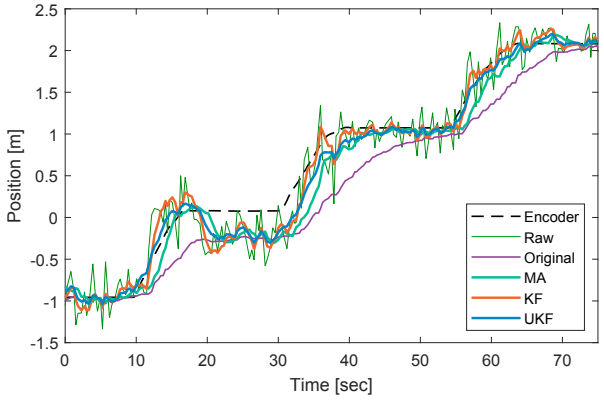

Fig. 9. Comparison of different filter algorithms applied on data from experiment with three stops, each stop has a duration of 14 sec.

tally evaluated. Results showed that the model-based filters provide lower filter lag compared to the model-free and the original filter. The UKF performed best in regards to convergence time. However, none of the filters could eliminate the sensor lag experienced in the raw signal. Input for the UKF is estimated from encoder measurements rather than from a thruster model. The results presented for the UKF, therefore, can be more precise than given for real system inputs. Further tests with actual thruster inputs need to be conducted to evaluate the true performance of the UKF. Furthermore, it is assumed that no rotation of the ROV occurs, which is reasonable in the specific case investigated in this study. But for scenarios where the ROV moves freely, this could be too restrictive. Extending the UKF to include angular position and velocities is left to future work, however, this requires accurate and reliable attitude measurements. The test shown in Fig. 9 showed that the acoustic reflection may have interfered with the SBL signal causing a position estimation error in areas of the pool. Similar issues are not expected in open-water tests, but should be subject for future work.

ACKNOWLEDGEMENTS

The authors would like to thank for the support from the Energy Technology Development and Demonstration Programme (EUDP) via the "ACOMAR – Auto Compact Marine Growth Remover" project (J.No. 64020-1093). Thanks also go to our project partners SubC Partner, Sihm Højtryk, Mati2ilt, Total E&P Denmark and Siemens Gamesa Renewable Energy.

REFERENCES

Benzon, M.S.R.v., Sørensen, F.F., Liniger, J., Pedersen, S., Klemmensen, S., and Schmidt, K. (2021). Integral sliding mode control for a marine growth removing rov with water jet disturbance.

Fossen, T.I. (2011). *Handbook of Marine Craft Hydrodynamics and Motion Control*. Wiley, Hoboken, 1. aufl. edition.

Jørgensen, E.K., Fossen, T.I., Bryne, T.H., and Schjølberg, I. (2020). Underwater position and attitude estimation using acoustic, inertial, and depth measurements. doi:10.1109/JOE.2019.2933883. ID: 1.

Kazimierski, W. and Zaniewicz, G. (2021). Determination of process noise for underwater target tracking with forward looking sonar. *Remote sensing (Basel, Switzerland)*, 13(5), 1014. doi:10.3390/rs13051014.

Kinsey, J.C., Eustice, R.M., and Whitcomb, L.L. (2006). A survey of underwater vehicle navigation : Recent advances and new challenges. *IFAC Conference of Manoeuvering and Control of Marine Craft*, 88, 1–12. URL `https://www.whoi.edu/cms/files/jkinsey-2006a_20090.pdf`.

Li, Q., Li, R., Ji, K., and Dai, W. (2015). Kalman filter and its application. In - *2015 8th International Conference on Intelligent Networks and Intelligent Systems (ICINIS)*, 74–77. doi:10.1109/ICINIS.2015.35. ID: 1.

Mai, C., Pedersen, S., Hansen, L., Jepsen, K.L., and Yang, Z. (2016). Subsea infrastructure inspection: A review study. In - *2016 IEEE International Conference on Underwater System Technology: Theory and Applications (USYS)*, 71–76. doi:10.1109/USYS.2016.7893928. ID: 1.

Mandt, M., Gade, K., and Jalving, B. (2001). Integrating dgps-usbl position measurements with inertial navigation in the hugin 3000 auv.

Manzanilla, A., Reyes, S., Garcia, M., Mercado, D., and Lozano, R. (2019). Autonomous navigation for unmanned underwater vehicles: Real-time experiments using computer vision. doi:10.1109/LRA.2019.2895272. ID: 1.

Park, S., Gil, M.S., Im, H., and Moon, Y.S. (2019). Measurement noise recommendation for efficient kalman filtering over a large amount of sensor data. doi:10.3390/s19051168.

Paull, L., Saeedi, S., Seto, M., and Li, H. (2014). Auv navigation and localization: A review. *IEEE Journal of Oceanic Engineering*, 39(1), 131–149. doi:10.1109/JOE.2013.2278891.

Pedersen, S., Liniger, J., Sorensen, F.F., and von Benzon, M. (2022). On Marine Growth Removal on Offshore Structures. In *Proceedings of the IEEE OCEANS 2022 conference*, 1–5. Chennai.

Pedersen, S., Liniger, J., Sørensen, F.F., Schmidt, K., von Benzon, M., and Klemmensen, S.S. (2019). Stabilization of a rov in three-dimensional space using an underwater acoustic positioning system. *IFAC PapersOnLine*, 52(17), 117–122. doi:10.1016/j.ifacol.2019.11.037.

Ribas, D., Ridao, P., Mallios, A., and Palomeras, N. (2012). Delayed state information filter for usbl-aided auv navigation. In *2012 IEEE International Conference on Robotics and Automation*, 4898–4903. doi:10.1109/ICRA.2012.6224989.

Sørensen, F.F., von Benzon, M., Liniger, J., and Pedersen, S. (2022). A quantitative parametric study on output time delays for autonomous underwater cleaning operations. *Journal of Marine Science and Engineering*, 10(6). doi:10.3390/jmse10060815.

Wallen, J. and Song, Z. (2019). Development of an adaptive docking station for resident underwater vehicles. In - *OCEANS 2019 - Marseille*, 1–7. doi:10.1109/OCEANSE.2019.8867444. ID: 1.

Wan, E.A. and Merwe, R.V.D. (2000). The unscented kalman filter for nonlinear estimation. In - *Proceedings of the IEEE 2000 Adaptive Systems for Signal Processing, Communications, and Control Symposium (Cat. No.00EX373)*, 153–158. doi:10.1109/ASSPCC.2000.882463. ID: 1.

WaterLinked (2022). Bluerov2 integration. URL `https://waterlinked.github.io/underwater-gps/integration/bluerov-integration/`.

Yang, Y. and Huang, G. (2017). Acoustic-inertial underwater navigation. In *2017 IEEE International Conference on Robotics and Automation (ICRA)*, 4927–4933. doi:10.1109/ICRA.2017.7989571.